Reaction Chemistry & Engineering

Predicting thermal excursions during in-situ oxidative regeneration of packed bed catalytic fast pyrolysis catalyst

Journal:	*Reaction Chemistry & Engineering*
Manuscript ID	RE-ART-01-2021-000007.R1
Article Type:	Paper
Date Submitted by the Author:	18-Mar-2021

Complete List of Authors:

Adkins, Bruce; Oak Ridge National Laboratory, Chemical Process Scale-up Group
Mills, Zachary; Oak Ridge National Laboratory, Chemical Process Scale-up Group
Parks, James; Oak Ridge National Laboratory, Chemical Process Scale-up Group
Pecha, Michael; National Renewable Energy Laboratory,
Ciesielski, Peter; National Renewable Energy Laboratory, Biosciences Center
Iisa, Kristiina; National Renewable Energy Laboratory, National Bioenergy Center
Mukarakate, Calvin; National Renewable Energy Laboratory, National Bioenergy center
Robichaud, David; National Renewable Energy Laboratory, Biosciences Center; NREL
Smith, Kristin; National Renewable Energy Laboratory
Gaston, Katherine; National Renewable Energy Laboratory
Griffin, Michael; National Renewable Energy Laboratory, National Bioenergy Center
Schaidle, Joshua; National Renewable Energy Laboratory, National Bioenergy Center

ARTICLE

Predicting thermal excursions during *in-situ* oxidative regeneration of packed bed catalytic fast pyrolysis catalyst

Received 00th January 20xx,
Accepted 00th January 20xx

DOI: 10.1039/x0xx00000x

Bruce D. Adkins,[a*] Zach Mills,[a] James Parks II,[a] M. Brennan Pecha,[b] Peter N. Ciesielski,[b] Kristiina Iisa,[b] Calvin Mukarakate,[b] David J. Robichaud,[b] Kristin Smith,[b] Katherine Gaston,[b] Michael B. Griffin[b] and Joshua A. Schaidle[b]

Ex-situ Catalytic Fast Pyrolysis (CFP) uses a secondary reactor to upgrade biomass pyrolysis vapors to stabilized CFP oils with reduced oxygen content. In one configuration, the secondary reactor is operated as a packed-bed swing reactor system which allows coke-deactivated beds to be decarbonized in-situ while other beds remain online for vapor upgrading. In-situ decarbonization must be done carefully to avoid irreversible deactivation and/or physical degradation of catalyst pellets. Given that packed bed reactors are well known to have poor heat transfer characteristics, this is a critical issue impacting scaleability and commercial viability of the techology. To predict thermal excursions during regeneration, finite element computational models have been built to assist in scaling up oxidative decarbonization of a Pt/TiO_2 CFP catalyst (0.5mm spheres) from a bench scale packed bed with 100 g of catalyst to a pilot scale packed bed with 2 kg of catalyst and internal cooling tubes. Based on transient measurements of outlet temperature and effluent CO_2 concentration, and using an assumed coke profile and activation energy, this paper demonstrates that specific combinations of effective thermal conductivity and wall heat transfer coefficient can fit bench scale oxidative regeneration data equally well. For the upscaled 2 kg bed, four bench-scale "best fit" parameter pairs give different predictions for location and magnitude of thermal excursions, with the maximum computed bed temperature gradients ranging from 30 ^oC/cm to as high as 3,000 ^oC/cm. The larger the fraction of heat removal by conduction through the cooling tubes, the greater the differences between the parameter pairs.

The modelling results presented in this paper cast doubt on the industrial viability of the proposed combination of catalyst, bed and regeneration process, and point to the need for alternate reactor designs. However, there is considerable uncertainly in some of the key model parameters. The reliability of model predictions can be increased by adding more temperature measurements at key bed locations, testing additional variations in process conditions, performing careful bed dissections to determine the true coke profile, and perhaps most importantly, directly measuring the effective thermal conductivity of the catalyst pellets.

Introduction

Catalytic Fast Pyrolysis (CFP) is an emerging technology to convert lignocellulosic biomass to fungible fuels and chemicals. In *ex-situ* CFP, biomass is fed into an anaerobic thermal pyrolyzer to generate pyrolysis vapors which are then transported into a second reactor to be cracked, partially deoxygenated and otherwise upgraded. The resulting CFP oil is more stable than raw pyrolysis oil and easier to process in finishing reactors. Options for finishing include a) standalone hydrotreating to produce fungible fuel blendstocks,[1, 2] b) co-processing with refinery streams in existing hydrotreaters, c) further processing into chemicals or materials[3, 4] and d) direct use as a fuel for heating or power generation. When bifunctional metal-acid catalysts such as Pt/TiO_2[1] or Mo/Al_2O_3[5] are used, hydrogen can be co-fed to the upgrading reactor to promote removal of oxygen as water.[1, 6] Hydrogen can also reduce light gas generation and formation of coke on the catalyst.[1, 3-5, 7-11]. This can increase carbon yield in the CFP oil and improve process resilience. Recently reported microreactor[6] and bench-scale work[1, 12] have shown particularly promising CFP oil yields for the specific case where pine was pyrolyzed in a fluidized bed reactor and the vapors were upgraded over a packed bed of Pt/TiO_2 catalyst, with co-fed H_2 at near atmospheric pressure. In light of these and other

[a.] *Oak Ridge National Laboratory, 1 Bethel Valley Rd, Oak Ridge, TN 37830*
[b.] *National Renewable Energy Laboratory, 15013 Denver W Pkwy, Golden, CO 80401*
* Corresponding author email adkinsbd@ornl.gov
† Electronic supplementary information (ESI) is available.

encouraging results, there is considerable interest in further technological development and process scale-up.[13]

Compared to circulating catalyst processes like FCC (fluid catalytic cracking), the packed bed process has advantages of simplicity and lower cost.[12] It also allows catalysts to reach much higher coke levels before regeneration, which can greatly reduce the number of regeneration cycles, potentially providing for longer catalyst lifetime. As well, it eliminates the particle-particle and particle-wall collisions that can lead to catalyst attrition. Avoiding attrition is especially important for catalyst components that are difficult to bind during spray drying (the technology by which all FCC catalysts are produced). However, all these advantages are moot unless the in-situ regenerations can be carried out under careful conditions that avoid thermal excursions. Thermal excursions can occur in any exothermic packed bed catalytic reactor, are almost always detrimental to catalyst activity, and can cause physical breakdown of the pellets located in or near the vicinity of thermal excursions. This in turn can lead to fines generation inside the reactor, which can plug outlet screens and other downstream hardware, causing premature shutdown and expensive turnarounds. Thus, thermal excursions must be carefully avoided to make exothermic packed bed processes commercially viable.

Another seeming disadvantage to the packed bed is that the entire catalyst bed must be taken offline to accomplish regeneration. However, swing cycle reactor systems (Figure 1) can circumvent this limitation, since one or more reactors are always online while others are being regenerated. Of course, cost dictates that the number of reactors be minimized. To meet this objective, the design of the swing cycle process must consider the onstream time (limited by rate of deactivation by coke) compared to the regeneration time. Reducing the regeneration time allows the total number of reactors to be reduced but increases the risk of thermal excursions during regeneration. Thus, the design of the swing process requires a full understanding of heat generation and transfer in the packed bed. Many variables come into play, including size, shape and composition of catalyst pellets; size and configuration of the catalyst beds; gas flows (oxygen and inert) and gas flow ramping; and the design and operation of hardware intended to cool the beds, either internally or through the reactor wall. As will be demonstrated, the amount and composition of coke is also of importance, as are the combustion kinetics and the distribution of coke throughout the reactor. In this paper, we deal only with axial variations in coke (in the direction of flow), which will be referred to as “coke profile.”

It is very well known, both in literature and widespread industrial practice, that the heat transfer characteristics of packed bed reactors are poor. Quantitative analyses of internal temperature gradients based on varying degrees of simplification of the coupled system of equations describing reaction, mass transfer and heat transfer have been in existence since the 1950’s. References 14 to 16 cite three seminal articles spanning a period of seventy years[14-16]. In particular, the

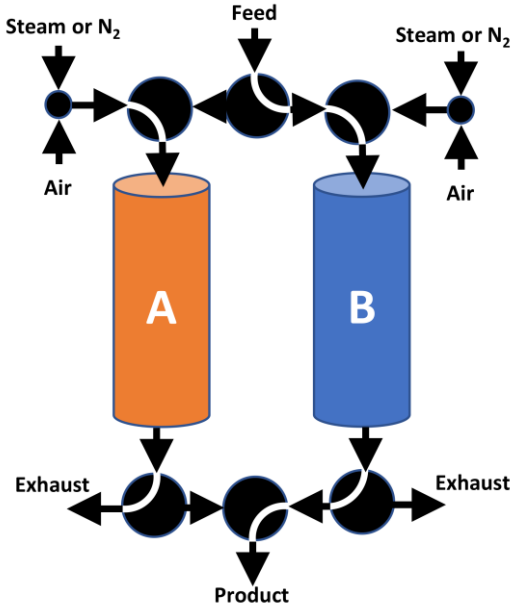

Figure 1. Simplified swing system with two reactors. Reactor A is in regeneration model and reactor B is in upgrading model.

methodologies of Hickman et.al[16], and the associated web tool made available to the public (appropriately named GradientCheck[17]) provide a concise quantitative analysis to test for the potential of gradients in packed bed catalytic reactors. Because one of the main reactants (coke) is a fixed, non-diffusing species, and regeneration is a transient process, Gradientcheck is not strictly applicable to the application studied in this paper. However, it still provides a very good starting point for the modelling work.

The main parameters affecting heat transfer in packed beds are the effective thermal conductivity of the catalyst pellets and the wall heat transfer coefficient. It has been known for decades that the effective thermal conductivity of porous particles can be much lower than the thermal conductivity of the matrix materials in bulk form[18-21]. The general explanation invokes the particulate nature of the solid. In most industrially produced porous pellets, primary crystalline or amorphous nanoparticles form larger agglomerates, which in turn form the solid matrix of the porous pellets. Conduction of heat through the matrix depends on the myriad of tiny contact points between the primary particles. The wall heat transfer coefficient is also complex: pellet shape, size distribution and packing all influence wall conduction, well as reactor geometry and wall roughness.

Of course, reaction kinetics and enthalpy changes also have a large impact on the thermal behavior of packed beds of catalyst. Additionally, pressure drop is always an important consideration, especially as it limits the flow of cooling gases. In most cases, hardware considerations will limit pressure drop(s) for the entire reactor system or for individual components. But even in the absence of equipment limits, pressure gradients must be kept far below the average crush strength of the

catalyst pellets, because weak pellets will always be present. For high temperature processes, the issue is doubly important; catalyst physical properties at elevated temperatures is a complex research area receiving limited attention.

The aim of this work was to construct and use a computational model to assess the viability of an in-situ regeneration process as a component in a cyclic packed-bed CFP process. Initial guidance for the study came from the GradientCheck web tool, which indicated that substantial gradients (particularly temperature) would exist in the catalyst beds. Even though GradientCheck is not strictly applicable to transient oxidative regeneration, the assessment led us to carry out the modelling study, and tailor it to address the most critical unknown parameters: the effective solids thermal conductivity and the wall heat transfer function. Two reactor systems were modeled: a bench scale unit for which some regeneration data was available, and a pilot scale unit representing the first scale-up step. Data from the bench scale unit was used to bound the critical parameters. Further reduction in the uncertainty of these parameters will required additional experimentation, as described in the summary.

Table 1. Important physical properties for TiO2 carrier

Parameter Name and Symbol		Units	Value	Ref.
Crystal phase		Anatase TiO_2		Ref 28
BET surface area	S_{BET}	m^2/g	54	
Hg pore volume	PV	cm^3/g	0.37	
Bulk loading density	ρ_b	kg/m^3	900	
Skeletal density	ρ_s		3900	Ref 29
Envelope pellet density	ρ_{pe}		1600	Eq. 10
Mean pore diameter	MPD	m	$2.7x10^{-8}$	Eq. 23
Pellet matrix volume fraction	θ_{pe}	-	0.408	Eq. 12
Pellet pore volume fraction	ε_{pe}		0.592	Eq. 11
Bed pellet volume fraction	θ_b		0.563	Eq. 13
Bed void volume fraction	ε_b		0.437	Eq. 14
Overall solid volume fraction	θ		0.230	Eq. 15
Overall void volume fraction	ε		0.770	Eq. 16
Pellet diameter, 10% passing	D_{10}	mm	0.490	Ref 28
Pellet diameter, 50% passing	D_{50}		0.509	
Pellet diameter, 90% passing	D_{90}		0.546	
Bulk heat capacity	c_p	J/(kg·K)	680	Ref 29
Bulk thermal conductivity	k_b	W/(m·K)	11.9	

Table 2. Other thermal parameters required for modelling

Parameter Name and Symbol	Units		Value
Carbon combustion enthalpy	H_c	J/mol	$3.94x10^5$
Combustion activation energy	E_a		$5x10^4$
Combustion frequency factor (surface reaction)	A_f	$m^3/(mol·s)$	Study Parameters
Wall heat transfer coefficient	h_w	$W/(m^2·K)$	
Effective thermal conductivity of solid matrix material	$k_{s,eff}$	W/(m·K)	

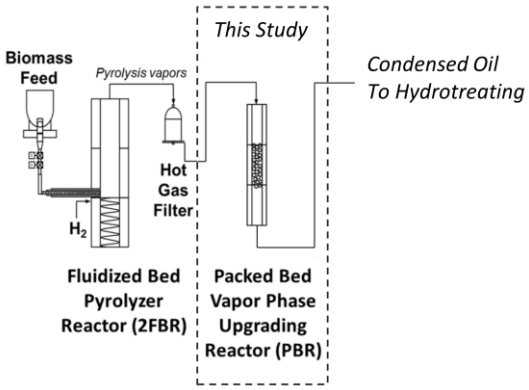

Figure 2. Schematic of the "2FBR" unit at NREL.

Methods and Approach

Key Catalyst and Thermal Parameters

Table 1 gives the important physical properties of the carrier pellets, assumed representative of all catalyst pellets in the packed beds. Table 2 summarizes additional thermal parameters important to this investigation. Three of these parameters - combustion pre-factor, effective solids thermal conductivity and wall heat transfer coefficient - are treated as study parameters, as no definitive values exist for this catalyst at the time of this writing. A fourth variable, activation energy, is also not known precisely for CFP coke, but a value of $5x10^4$ J/mol typical for a "soft petroleum coke" was deemed a reasonable choice for this study[22]. While on the low side for combustion, it is consistent with unpublished industrial values used by the lead author for modelling pilot-plant FCC regenerators, ranging between $5x10^4$ J/mol for "soft" coke to $1.3x10^5$ J/mol for "hard" coke. The "hard-soft" distinction is based on hydrogen content, heteroatom content, fraction of carbon in polynuclear aromatic rings, and combustion behavior. Time and equipment limitations did not allow combustion kinetic studies be carried out in the bench scale reactor system, so the chosen value of activation energy should be regarded as an educated guess.

Bench Scale Reactor System

The experiments used to provide regeneration data for model development were performed in a bench scale *ex-situ* CFP system consisting of a 5.08 cm id bubbling bed pyrolysis reactor coupled in series to a 3.48 cm id packed bed reactor (PBR) loaded with ca. 100 g of Pt/TiO_2 catalyst, with a nominal bed depth of 11.7 cm. This system, located at the National Renewable Energy Laboratory (NREL) and known as the "2FBR", is illustrated in Figure 2. Briefly, the pyrolysis reactor uses a bubbling bed of sand fluidized with an 85 v% H_2 15 v% N_2 gas mixture at near atmospheric pressure (roughly 82 kPa in Golden CO) at a nominal flowrate of 16 SLPM, temperature of 500°C and biomass feedrate of 150 g/hr. Pyrolysis vapors and gases leave the fluidized bed reactor and flow into the loaded PBR.

Vapor upgrading continues until the catalyst is deactivated to a minimal level of activity, at which point the bed is stripped in flowing N_2, regenerated in an N_2/air mixture (also at nominal 16 SLPM) and finally reactivated in flowing H_2 before starting the next upgrading cycle. Wall temperatures during regeneration are maintained at 400-410°C; however, significant temperature variations usually occur within the bed. Reactor outlet temperature is measured with a thermocouple located at the center of a metal screen supporting the catalyst bed. Because the metal screen can have an averaging effect on measured outlet temperature, this study compares both average and center point modelled temperatures with measured temperatures.

Since there is only one upgrading reactor in the 2FBR system, true swing cycle operation is not possible. Instead, the upgrading reactor is cycled by shutting off biomass feed and switching gas streams. The effect of cycling the pyrolyzer is not believed to be detrimental to simulated swing operation of the upgrading reactor.

Figure 3 shows an example of flowrate and temperature data for the regeneration step in the 2FBR system. To keep temperature under control, the composition of the regeneration gas (N_2 + air) in this unit is always kept below 1 v% O_2. This limit is based on experience and is consistent with guidelines for in-situ oxidative regeneration of coke deactivated industrial scale packed bed reactors.[23] The amount of coke on catalyst (g carbon per g fresh catalyst) is estimated by integrating the CO_2 produced during the regeneration step, after baseline correction if necessary. CO production is usually absent from the effluent stream. Experimental coke levels on catalyst range between 15 w% and 25 w% % (g carbon per g fresh catalyst), depending primarily on the quantity of pyrolysis vapors flowed over the catalyst (expressed as biomass to catalyst mass ratio, or B/C). Because of the high B/C (12) and coke level (25 w%), the data shown in Figure 3 was used for this study to represent the extreme case.

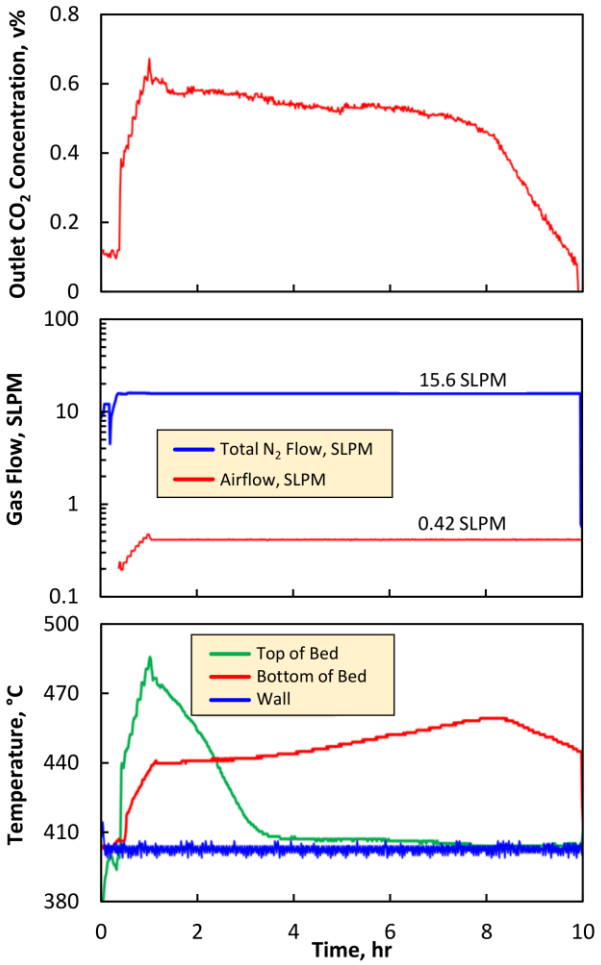

Figure 3. Experimental regeneration conditions from the selected 2FBR run. Top: vol% CO_2 in reactor effluent. Middle: inlet gas flowrates (in standard liters per minute) of N_2, H_2 and air. Note the logarithmic scale. Bottom: temperatures at top of bed, bottom of bed and reactor wall.

Pilot Scale CFP System

The target unit for the scaleup exercise is the Thermal and Catalytic Process Development Unit (TCPDU), also located at NREL. The layout is similar to the 2FBR, but there are a number of differences. Most important for this study, there are three existing cylindrical reactors consisting of 145 mm ID, 1525 mm long tubular vessels, each with three internal heating rods (24.8 mm OD) that can be converted to cooling tubes. In this study, we examine an overall scaleup factor of 60 using the same WHSV as the 2FBR unit (1.5 hr^{-1}): 9 kg/hr of biomass and 6 kg of the Pt/TiO_2 catalyst.

The maximum pressure drop of the entire TCPDU system limits the pressure drop across the catalyst bed to 20 kPa or less. Because the small pellet size of the catalyst used in this study results in large pressure gradients, catalyst beds in the existing reactors are limited to 3 kg or less. Since three reactors were available, the decision was made to model the process with the catalyst divided uniformly between them, to minimize pressure drop and improve heat removal. In this configuration, all three reactors would be online at the same time, and the operation would be more or less identical to the 2FBR, in that the operating cycle will require regular interruptions to biomass flow. The perceived downside of this mode of operation is small and easily outweighed by the need to preserve adequate control margins for pressure drop and bed temperatures.

Even with 2 kg beds, nitrogen flow during regeneration is capped at 400 SLPM per catalyst bed (1200 SLPM for all 3 beds) to maintain an adequate pressure drop control margin. To assist in removing the heat of regeneration, the concept calls for converting the bayonet rods to cooling tubes and leaving the outer wall insulated by heating blankets. These blankets will provide any heat necessary during upgrading but will only be operated as needed to eliminate heat loss through the wall during regeneration. This approach is intended to mimic

industrial practice with large catalyst beds having negligible wall heat transfer. The wall thickness of the cooling tubes is 1.9 mm, leaving the inner diameter at 21.0 mm. The cooling tube material is specified as AISI 4340 steel. The thermal properties of the steel were taken from a commercial software (COMSOL) materials database. Air at 30°C was selected as the cooling medium. Maximum airflow was set at 200 SLPM per tube (600 SLPM per bed, 1800 SLPM for all three catalyst beds). This limit is set by the availability of compressed air in the TCPDU facility.

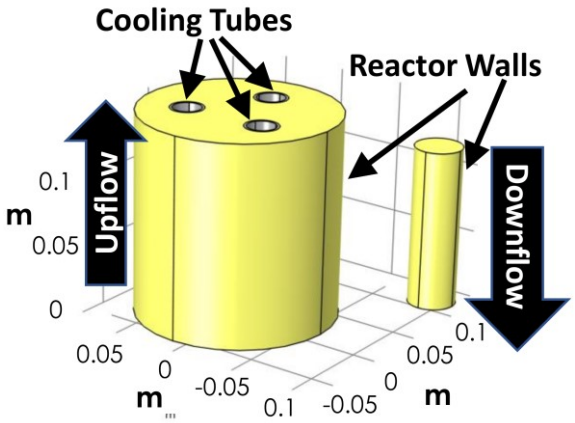

Figure 4. Left: TCPDU-PBR pilot scale catalyst bed with 2 kg of catalyst and 3 internal cooling tubes. Catalyst is light yellow and cooling tubes are gray. When loaded with 2 kg of the catalyst in Table 1, the bed diameter is 14.5 cm and bed depth is 14.7 cm. Right: 2FBR-PBR bench scale catalyst bed loaded with 100 g catalyst. Bed diameter is 3.48 cm and bed depth is 11.7 cm.

Gradientcheck Analysis

Figure 4 shows illustrations of the 2 kg pilot scale catalyst bed (left side), including the three cooling tubes, and the 100 g bench scale catalyst bed (right side).

The GradientCheck[17] web tool was used to assess the likelihood of axial and (especially) radial gradients in the catalyst beds. Two GradientCheck reports can be found in the Electronic Supplemental Information (ESI), in Figures S1 and S2. The most important inputs are tabulated in Table 3. Other inputs listed in Figures S1 and S2 are taken from Tables 1 and 2.

Table 3. Input parameters for GradientCheck

Parameter	Units	2FBR-PBR	TCPDU-PBR
Temperature	°C	410	
Pressure	Pa	90,000	
Catalyst	kg	0.100	20.0
Bed radius	m	0.0174	0.0725
Bed length	m	0.1168	0.135*
Initial carbon	kg/kg.cat	0.25	
Initial carbon	mol	2.08	41.6
Reaction rate	mol/kg.cat·s	6.42e-4	
O_2 conc.	mol%	0.55	
Fluid viscosity	kg/m.s	3.2e-5	
Fluid heat cap.	J/kg.K	1100	
Fluid therm.cond	W/m.K	5e-2	

* base case evaluation without cooling tubes

Table 4. Important outputs from GradientCheck

Parameter	Units	2FBR-PBR	TCPDU-PBR
Thiele modulus	-	3.8	
Effectiveness factor	-	0.24	
Pellet surface Δconc.	%	3.4	
Pellet surface ΔT	°C	0.08	
Pellet internal ΔT	°C	0.003	
Radial k_{eff}	W/m.K	0.14	
Axial ΔT	°C	125	2130
Does pore diffusion strongly affect rate?		Yes	
Does axial dispersion strongly affect rate?		Yes	
Do large radial bed temp gradients exist?		Yes	

The most Important outputs from GradientCheck are shown in Table 4. Summarizing:

- Diffusion in the pellets has a strong, rate limiting effect.
- Heat transfer inside the pellets is much faster than at the particle surface, so the pellets are essentially isothermal. (The same conclusion is reached by estimating the range in Biot numbers of these pellets, which are generally much lower than unity.)
- Heat transfer through the bed (between the particles) and through the wall is limiting, resulting in very high axial and radial temperature gradients, which strongly affect the overall reaction rate.
- The predicted axial temperature increase for the TCPDU bed is extremely high.

Temperatures are the most concerning of these predictions, especially for the TCPDU bed. Since GradientCheck does not strictly apply to this regeneration case, these results led us to undertake the model development work reported in this paper, with a focus on effective solids thermal conductivity and wall heat transfer coefficient. The predicted effectiveness factors warrant that the model combines both reactor-scale and particle-scale mass and heat transport effects.

Model Description

Two finite element model geometries were constructed: one for the 2FBR PBR, and one for the TCPDU PBR. Because the 2FBR PBR is a simple cylinder, the modelled geometry is a 2D half cross section with an axis of symmetry on the centerline. Because of the cooling tubes, the TCPDU model requires full 3D geometry, but the 3-fold symmetry allows the computational domain to be reduced to a one-third pie-slice segment with symmetry boundary conditions at all vertical segment faces.

Pellet interior. A single "extra dimension" is created in the computational domains to represent the interiors of the porous catalyst pellets, as illustrated in Figure 5. Nonspherical pellets can be accommodated using the spherical-equivalent radius r_{pe} defined as:

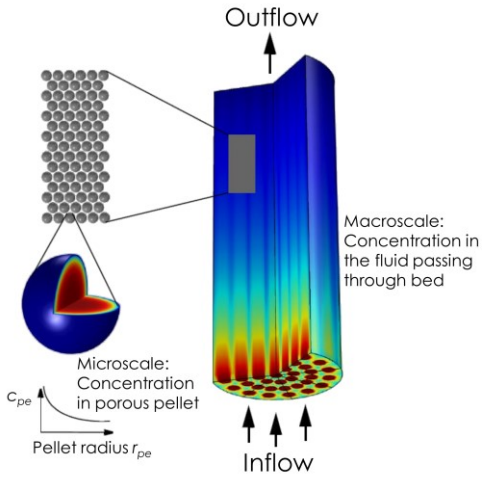

Figure 5. Use of the extra dimension to compute variables in the pellet interior for a packed bed of catalyst similar to the ones in this study. Colors represents concentrations of reactant. Image made using COMSOL Multiphysics® software and is provided courtesy of COMSOL.[30]

$$(1)\quad r_{pe} = 3\frac{V_{pe}}{A_{pe}}$$

where V_{pe} and A_{pe} are the envelope volume and envelope surface area of a single pellet. Using this definition of r_{pe}:

$$(2)\quad S_b = \frac{3}{r_{pe}}(1-\varepsilon_b)$$

where S_b is external (envelope) surface area of pellets per unit volume of bed and ε_b is bed void fraction.

The shell balance for species *i* at radial position *r* inside the spherical catalyst pellet is:

$$(3)\quad 4\pi N\left\{r^2 r_{pe}^2 \varepsilon_{pe}\frac{\partial}{\partial t}\left(c_{pe,i}\right) + \nabla\cdot\left(-r^2 D_{pe,i}\nabla c_{pe,i}\right)\right\} = r^2 r_{pe}^2 R_{pe,i}$$

where r is the dimensionless position inside the pellet (r_{pos}/r_{pe}), ε_{pe} is the void fraction inside the pellet, $c_{pe,i}$ is the molar concentration of species *i* inside the pellet, $D_{pe,i}$ is the diffusivity of species i inside the pellet, $R_{pe,i}$ is the reaction rate of species *i* per unit volume of pellet, and N is the number of pellets per unit volume of bed. Zero advection is assumed inside the pellets. The following equation describes the mass flux at the external surface of the pellets:

$$(4)\quad \varepsilon_b\frac{\partial c_i}{\partial t} + \mathbf{u}\cdot\nabla\mathbf{c_i} + \nabla\cdot(-\mathbf{D_i}\nabla\mathbf{c_i}) = R_i - S_b h_{c,i}\left(c_i - c_{pe,i}\right)$$

where $h_{c,i}$ is the surface mass convection coefficient for species *i*, c_i is the bulk molar concentration of species *i*, D_i is the bulk diffusivity of species *i*, R_i is the reaction rate of species *i* per unit bed volume and **u** is the superficial fluid velocity vector. The surface mass convection coefficient can be determined from the Sherwood, Reynolds and Schmidt numbers:

$$(5)\quad \mathrm{Sh} = \frac{h_c d_{pe}}{D} \qquad (6)\quad \mathrm{Re} = \frac{\rho u d_{pe}}{\mu} \qquad (7)\quad \mathrm{Sc} = \frac{\mu}{\rho D}$$

where d_{pe} is pellet diameter ($2r_{pe}$), μ is the fluid dynamic viscosity and ρ is the fluid density. Sh can be related to Re and Sc using the relation developed by Frossling:[24]

$$(8)\quad \mathrm{Sh} = 2 + 0.552\,\mathrm{Re}^{1/2}\mathrm{Sc}^{1/3}$$

Finally, the mass conservation equation for bulk species *i* at every point in the bed is:

$$(9)\quad \varepsilon_b\frac{\partial c_i}{\partial t} + \mathbf{u}\cdot\nabla\mathbf{c_i} + \nabla\cdot\left(-\mathbf{D_{b,i}}\nabla\mathbf{c_i}\right) = R_i$$

Discretization of the particle interior is specified as the element count n_e in the extra dimension. This value is constant for all virtual pellets in the domain.

Volume fractions. The following equations relate volume fractions of solids and voids to pore volume *PV*, pellet (envelope) density ρ_{pe}, bed density ρ_b and skeletal density ρ_s. First**, inside the pellets**, θ_{pe} is the volume fraction of skeletal matrix and ε_{pe} is the volume fraction of pores.

$$(10)\quad \rho_{pe} = \frac{1}{PV + \frac{1}{\rho_s}}$$

$$(11)\quad \varepsilon_{pe} = PV\cdot\rho_{pe} \qquad (12)\quad \theta_{pe} = 1-\varepsilon_{pe}$$

At **bed scale**, θ_b is the volume fraction of pellets (using envelope volumes) and ε_b is the volume fraction of voids.

$$(13)\quad \theta_b = \frac{\rho_b}{\rho_{pe}} \qquad (14)\quad \varepsilon_b = 1-\theta_b$$

And finally, at **full reactor scale**, θ is the volume fraction of all solids in the reactor and ε is the volume fraction of all pores and voids.

$$(15)\quad \theta = \theta_b\cdot\theta_{pe} \qquad (16)\quad \varepsilon = 1-\theta$$

Virtual pellets. The "extra dimension" approach does not attempt to discretize all catalyst pellets in their specific positions, as this approach would be extremely expensive computationally. Instead, a virtual pellet is created in each grid cell. Used in combination with S_b (Equation 2), these virtual pellets represent the total mass and energy flows from the real pellets that would be located in each grid cell. Since each virtual pellet represents some number of real pellets, it is important to determine the effect of "pellet resolution" p_r defined as:

$$(17)\quad p_r = \frac{n_{pel}}{n_c}$$

where n_{pel} is the number of actual catalyst pellets and n_c is the number of grid cells.

Coke profile. Of great importance to this study is the capability to use space-dependent variables to define the initial concentrations of coke in the bed. This allows a non-uniform coke profile to be modelled. The importance of this capability cannot be overstated, because nonuniform coke profiles are commonly found in spent catalyst beds. In practice, coke profiles must be measured experimentally using bed dissection methods; however, that capability was not available on the

2FBR system. For this reason, we have substituted the coke profile from a recently published Pt/TiO_2 upgrading kinetics model[13] which was developed for the same catalyst and reactor. Figure 6 shows the coke profile predicted by the Pt/TiO_2 model for the same upgrading conditions used in the test shown in Figure 3. The output from the model are the discrete points (yellow circles), shown in normalized form (local coke concentration divided by average coke concentration). A simple equation was found to fit these values very well:

$$(18)\ CM = \frac{CB \cdot e^{-CB \cdot x}}{1 - e^{-CB}}$$

where *x* is the dimensionless position along the reactor axis, *CM* is the local coke multiplier and *CB* a parameter describing the magnitude of the variation in coke concentration. From this prediction, *CB*=1.8779 gives an excellent fit, shown as a gray line in Figure 6. Equation 18 is used as input to the model for specifying the local surface concentration of coke. This approach works equally well for surface and volumetric coke concentrations.

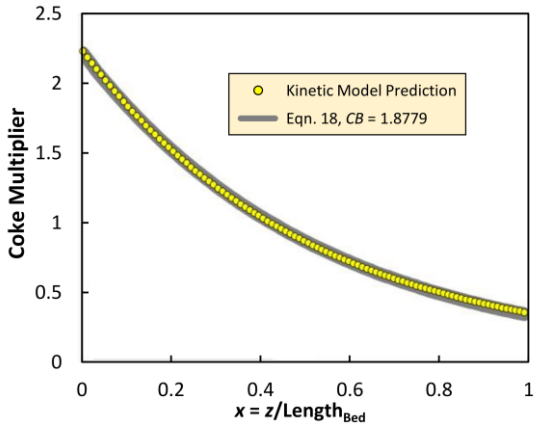

Figure 6. Normalized coke concentration (local concentration divided by average concentration) versus dimensionless position along the reactor axis. Yellow points are discrete values predicted by the Pt/TiO_2 kinetics model[13] and the gray curve is the simplified curve fit.

Carbon combustion. To allow future versions to incorporate changes in pore diameter caused by coke deposition, coke is represented as a surface species. (Note that the current version of the model uses a constant pore size based on the fresh catalyst.) For coke, there is no transport, so the conservation equation inside the pores is simply:

$$(19)\ \frac{\partial c_{pe,c}}{\partial t} = R_{pe,c}$$

The reaction is simple: surface carbon combines with oxygen to form carbon dioxide $C_{surf} + O_2 \rightarrow CO_2$. Since no CO has been observed in the bench scale experiments, partial combustion to CO is not included in the model. Some early simulations included hydrogen in the coke at levels typically seen in FCC cokes, but these resulted in overestimated heats of combustion and excessively high bed temperatures. At this stage of model development, hydrogen in coke is ignored.

Temperature dependence of the coke combustion rate is described with the Arrhenius equation:

$$(20)\ R_{pe,c} = c_{pe,c} c_{pe,O_2} . A_f \cdot e^{\left(-\frac{E_a}{R \cdot T}\right)}$$

where $c_{pe,c}$ and $c_{pe,O2}$ are concentrations inside the pellet, A_f is the frequency factor and E_a is the activation energy. For surface carbon with concentrations expressed as mol/m^2, A_f is still expressed in volumetric terms (m^3/(mol.s)), because the model uses S_{pe}, the specific internal surface area per envelope volume of pellet (m^2/m^3), to convert internally:

$$(21)\ S_{pe} = \frac{S_{BET} \cdot \rho_b}{\theta_b}$$

where S_{BET} is the BET surface area.

Thermodynamic properties of gases. A commercial software (COMSOL) thermodynamic database is used to estimate the physical properties of gases (O_2, CO_2 and N_2) and mixtures. For densities, gases are assumed ideal. Thermal conductivities are estimated using kinetic theory, and the Brokaw mixture rule is used to estimate viscosities. The only property not taken directly from COMSOL thermodynamics is diffusivity inside the catalyst pores. Instead, this was estimated using the Knudsen equation:[21]

$$(22)\ D_{ki} = \frac{MPD}{3} \sqrt{\frac{8RT}{\pi MW_i}}$$

where *R* is the gas constant (8.3144 J/(mol.K)), MW_i is the molecular weight of species *i*, *T* is temperature and *MPD* is the median pore diameter. *MPD* can be calculated from internal surface area and pore volume:

$$(23)\ MPD = \frac{4 \cdot PV}{S_{BET}}$$

Further reductions in diffusivities are due to the volume fraction of solid matrix and the tortuosity of the catalyst pore structure. For this, the relation of Millington and Quirk is used:[22]

$$(24)\ D_{pe,ki} = \varepsilon_p^{4/3} D_{ki}$$

Heat transfer. Heat transfer in the porous catalyst bed is modelled assuming heat conduction through parallel paths - the matrix solid and the fluid-filled voids - as well as advection from fluid flow. For simplicity, the porous medium is defined using the reactor-level solid and void fractions. The corresponding heat transfer equation is:

$$(25)\ \left(\rho C_p\right)_{eff} \cdot \frac{\partial T}{\partial t} + \rho_f C_{p,f} \boldsymbol{u} \cdot \nabla T + \nabla k_{eff} \nabla T = Q$$

where ρ_f is the fluid density, $C_{p,f}$ is fluid heat capacity, $(\rho C_p)_{eff}$ is the effective volumetric heat capacity of solid matrix and fluid phases defined by an averaging model, k_{eff} is the effective thermal conductivity of combined solid matrix and fluid phases, and *Q* is the heat source or sink. Radiative heat transfer is neglected.

The averaging model used for the two effective (solid + fluid) terms is a simple volume average using the reactor-level volume fractions θ and ε from Equations 15 and 16. For simplicity, no distinction is made between heat transfer inside pellets (with very small voids) and heat transfer between pellets (with much larger voids). Since the model treats pellets as isothermal, this assumption is reasonable, especially given the large degree of uncertainty in the solid phase thermal conductivity.

$$(26)\quad \left(\rho C_p\right)_{eff} = \left(\rho_s C_{p,s}\right)\cdot\theta + \left(\rho_f C_{p,f}\right)\cdot\varepsilon$$

$$(27)\quad k_{eff} = k_{s,eff}\cdot\theta + k_f\cdot\varepsilon$$

Equation 26 is trivial, but the value of $k_{s,eff}$ in Equation 27 is not. Given the importance of this parameter exemplified by the Gradientcheck analysis, its value must be treated as a variable and studied parametrically.

The wall heat transfer coefficient is also treated as a study parameter. In the pilot scale bed with cooling rods of 1.9 mm wall thickness, there are three conductances in series to consider. The first, at the interface between catalyst pellets and the wall, is modelled as a thin resistive layer with conductance equal to an assumed wall heat transfer coefficient h_w. The second conductance is through the metal tube wall, and the third at the inner tube wall in contact with the cooling gas. The third conductance makes use of a model for forced convection inside a tube, from Incropera and Dewitt:[27]

$$(28)\quad q_0 = h\,(T_{cool} - T)$$

where T is the (variable) inner wall temperature and T_{cool} is the temperature of the incoming cooling gas. The heat transfer coefficient h is calculated from:

$$(29)\quad h = 3.66\frac{k}{D} \qquad \mathrm{Re}_D \le 2500$$

$$(30)\quad h = 0.027\mathrm{Re}_D^{0.8}\mathrm{Pr}^{0.4}\left(\frac{\mu}{\mu_s}\right)^{0.14} \qquad \mathrm{Re}_D > 2500$$

$$(31)\quad \mathrm{Pr} = \frac{\mu C_p}{k} \qquad (32)\quad \mathrm{Re}_D = \frac{\rho u D}{\mu}$$

where D is tube diameter, Pr is the Prandtl number for the fluid, Re_D is tube Reynolds number, k is the fluid thermal conductivity, μ_s is the viscosity at inner tube wall temperature T and μ is the viscosity evaluated at $(T+T_{cool})/2$. An advantage of this treatment is that it is not necessary to estimate inner or outer tube wall temperatures.

Laminar flow and pressure drop. Using the Navier-Stokes momentum equation with no turbulence model:

$$(33)\quad \rho_f\frac{\partial \mathbf{u}}{dt} + \rho_f(\mathbf{u}\cdot\nabla)\mathbf{u} = \nabla\cdot[-p\mathbf{I} + \boldsymbol{\tau}] + \mathbf{F}$$

where ρ_f is fluid density, p is pressure, $\boldsymbol{\tau}$ is the viscous stress tensor, **F** is the volume force vector and **I** is the identity tensor. For a porous bed, the particle size and void fraction are used in place of the reactor diameter in Equation 33. To compute the pressure gradient, the Ergun equation is used. This equation has terms for both viscous and inertial pressure drop contributions, and has been proven accurate over wide ranges of velocities and pressure gradients:

$$(34)\quad -\nabla p = \frac{150\mu(1-\varepsilon_b)^2}{d_{pe}^2\varepsilon_b^3}\mathbf{u} + \frac{1.75\rho_f(1-\varepsilon_b)}{d_{pe}\varepsilon_b^3}\mathbf{u}|\mathbf{u}|$$

Results and Discussion

Discretization Tests

Pellet resolution. Discretization tests were carried out using both models to establish standard values of pellet resolution p_r and number of intraparticle elements n_e. Figures 7 and 8 show the results of varying p_r in the 2FBR bench-scale model (Figure 7) and TCPDU pilot-scale model (Figure 8). The TCPDU simulations use case 7 from Table 6, which has the lowest N_2 flow (200 SLPM), highest cooling air flow (600 SLPM) and steepest gradients. All simulations shown in Figures 7 and 8 used the same number of internal elements, n_e = 10. At this value, the workstation memory (RAM) of 1 TB set the limit on number of grid cells in the TCPDU finest grid simulation. Obviously an even finer grid could be computed by reducing n_e, but that would compromise the pellet resolution test.

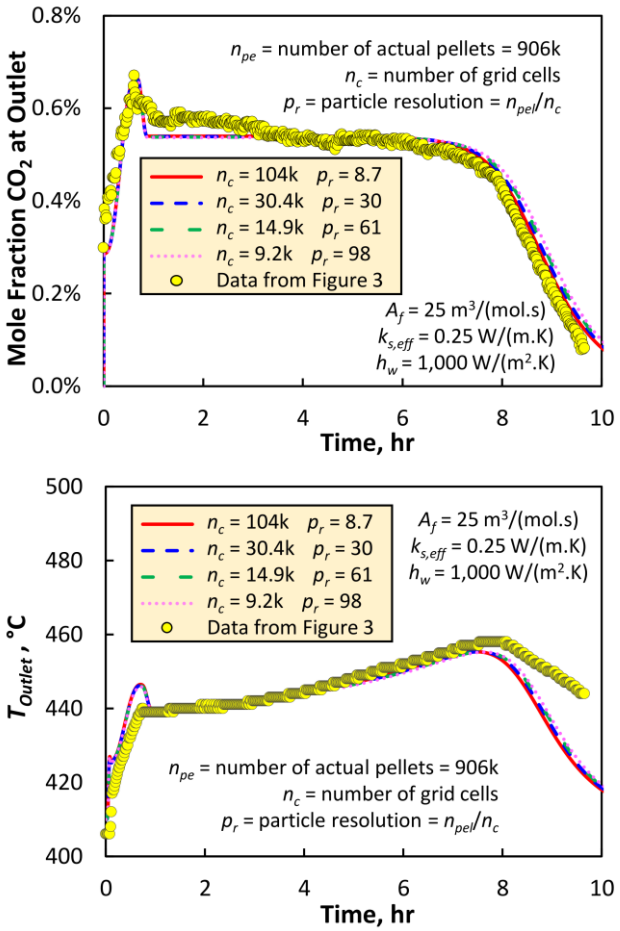

Figure 7. Experimental and modelled CO_2 (top) and temperature (bottom) profiles for the 2FBR bench scale reactor using four different pellet resolutions.

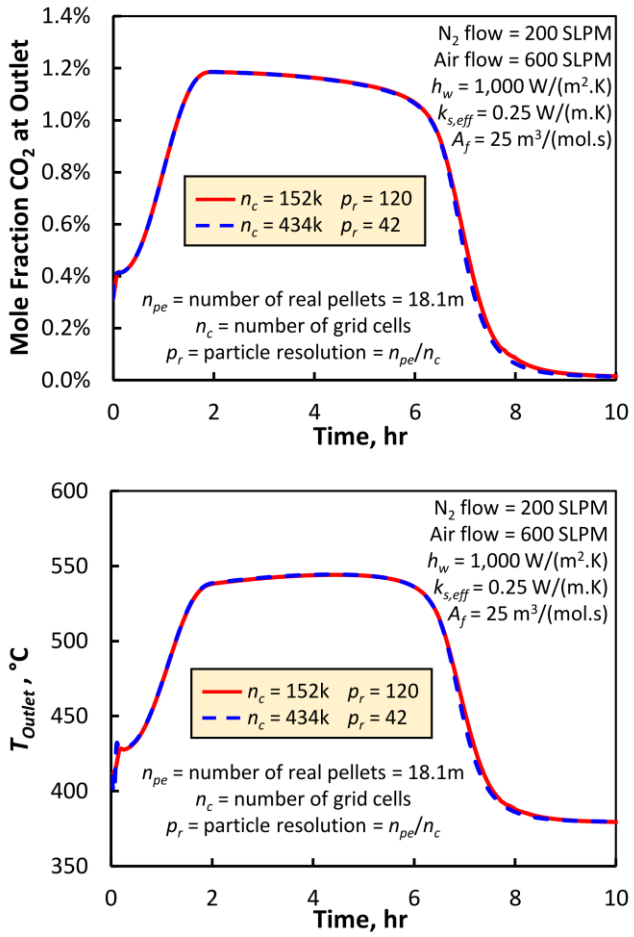

Figure 8. Experimental and modelled CO_2 (top) and temperature (bottom) profiles for the TCPDU pilot scale reactor using two different pellet resolutions.

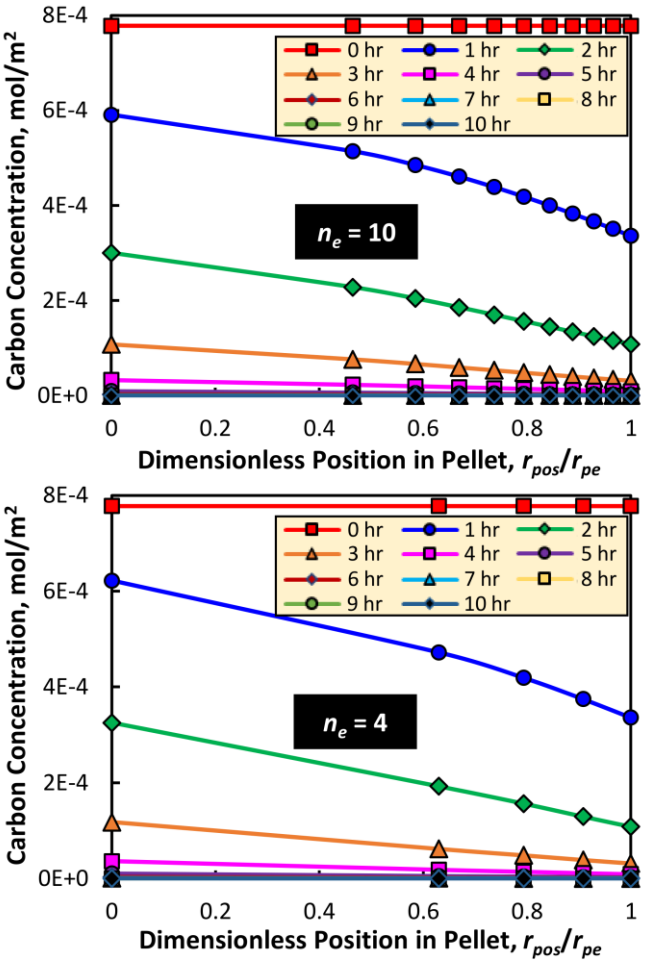

Figure 9. Coke concentration profiles inside a catalyst pellet located at dimensionless axial and radial bed positions x = 0.05 and r_b = 0.05, for high (n_e = 10, top) and low (n_e = 4, bottom) intraparticle element counts. The simulation uses the same thermal parameters shown in Figure 7. The time interval between curves is one hour.

While some negligibly small differences are visible in modelled CO_2 and outlet temperature profiles for both models, these tests confirm that pellet resolutions between 8.7 and 120 give essentially equal results.

Number of internal elements n_e. In finite element modelling, it is important to resolve gradients accurately to avoid nonphysical swings in concentrations that can lead to mass balance errors. Figure 9 shows two sets of intrapellet carbon concentration profiles for a pellet located at x = 0.05, r_b = 0.05 in the 2FBR catalyst bed. Pellets in other positions were also inspected: because of the initial coke profile, they showed differences in the level of coke concentrations, but were otherwise very similar to Figure 9. The upper graph shows the hourly coke profiles computed using the standard number of internal elements ($n_e = 10$), compared to a lower number (n_e = 4) in the lower graph. There were essentially no differences in mass balances, predicted CO_2 profiles, or outlet temperature profiles for these two cases. For safety, given that many of the TCPDU pilot-plant simulations showed higher temperatures and narrower combustion zones, the standard value of n_e was fixed at 10. To ensure this value was sufficient throughout the study, mass balances and intrapellet profiles were inspected for each simulation.

Keep in mind the curves in Figure 9 are not "snapshot" fluid-phase concentration profiles, but rather, the uncombusted carbon remaining at every hour on stream. Judging from the shapes of these coke profiles, the carbon combustion reaction is clearly diffusion limited, just as predicted by GradientCheck.

Table 5. Standard discretization parameters

Parameter		Units	2FBR	TCPDU
Grid cells	n_c	-	$104x10^3$	$152x10^3$
Avg cell length	-	mm	0.14	1.7
Real pellets	n_{pel}	-	$906x10^3$	$18.1x10^6$
Pellet resolution	p_r	-	8.7	120
Internal elements	n_e	-	10	

Table 5 gives the standard discretization parameters used in this computational study.

2FBR Bench Scale Model Fitting

The 2FBR regeneration model was fitted to the regeneration data in 3 using the parameters given in Tables 1 and 2 and the

coke profile shown in Figure 6 and Equation 18. The amount of coke, obtained by integrating the baseline-corrected CO_2 profile, was 25 w% (fresh catalyst basis). Inlet and wall temperatures were fixed at 410°C for the entire regeneration period of 10 hours. Modelled N_2 and air flow closely duplicated the experimental flows shown in 3. In all cases, gas flow was directed down the reactor. Referring back to Figure 6, the coke concentration decreases with distance down the reactor. As a result, the predicted combustion zone (the zone corresponding to complete consumption of O_2) becomes broader as the combustion front proceeds down the reactor.

Parametric sweeps were computed by varying the three study parameters shown in Table 2. Only simulations with carbon and oxygen balances between 99.5 and 100.5% were used. Mass balances falling outside this range mainly corresponded to low combustion rates, resulting in uncombusted carbon at the end of the simulations.

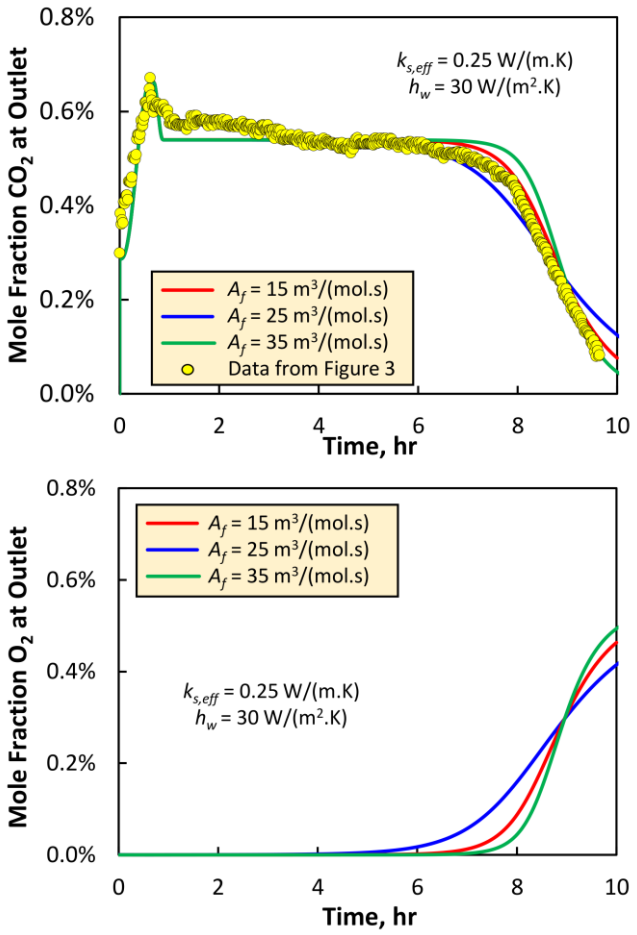

Figure 10. Experimental and modelled CO_2 (top) and modelled O_2 (bottom) effluent concentration profiles for 2FBR, for three different frequency factors.

The top graph in Figure 10 compares the outlet CO_2 transient profile from the reference run with three model simulations using different frequency factors: A_f = 15, 25 and 35 m³/(mol.s). In this simulation set, $k_{s,eff}$ and h_w were fixed at 0.25 W/(m.K) and 30 W/(m².K) respectively. This low value of $k_{s,eff}$ is consistent with literature examples cited earlier. Before reaching 5 hours, the three simulations are identical and flat. The reason, as shown in the bottom graph in Figure 10, is that oxygen consumption is 100%. Beyond 5 hours, the three simulations in Figure 10 diverge, because the leading edge of the combustion zone has passed the end of the catalyst bed, and oxygen consumption is no longer 100%. Importantly, this region of declining CO_2 concentration is the only region where reaction rates and kinetic parameters can be differentiated. Visibly, 25 m³/(mol.s) is a reasonable choice to fit the experimental data.

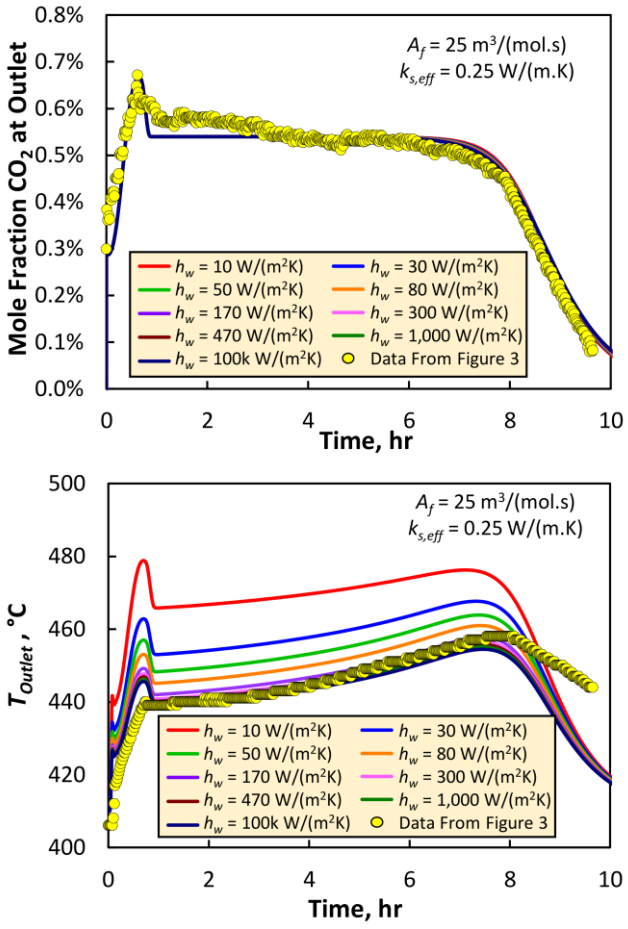

Figure 11. Experimental and modelled outlet temperature (top) and outlet CO_2 concentration (bottom) transient profiles for 2FBR simulations for different wall heat transfer coefficients.

In Figure 11, the experimental and modelled outlet temperature and CO_2 concentration profiles are compared for different values of wall heat transfer parameter h_w, for A_f = 25 m³/(mol.s) and $k_{s,eff}$ = 0.25 W/(m.K). As h_w is increased, the modelled outlet temperature decreases (top graph), but only to a point: above h_w = 470 W/(m².K), there is no difference. For simplicity, the value h_w = 1,000 W/(m².K) is paired with $k_{s,eff}$ = 0.25 W/(m.K) to create the first best-fit parameter pair. The bottom graph in Figure 11 also shows that there is no difference in the modelled CO_2 transient profile for any of the values in h_w. In fact, in more than 100 2FBR regeneration simulations with

the same activation energy (E_a = 5 x 10^4 J/mol), A_f was the only parameter having a real effect on the modelled CO_2 profile.

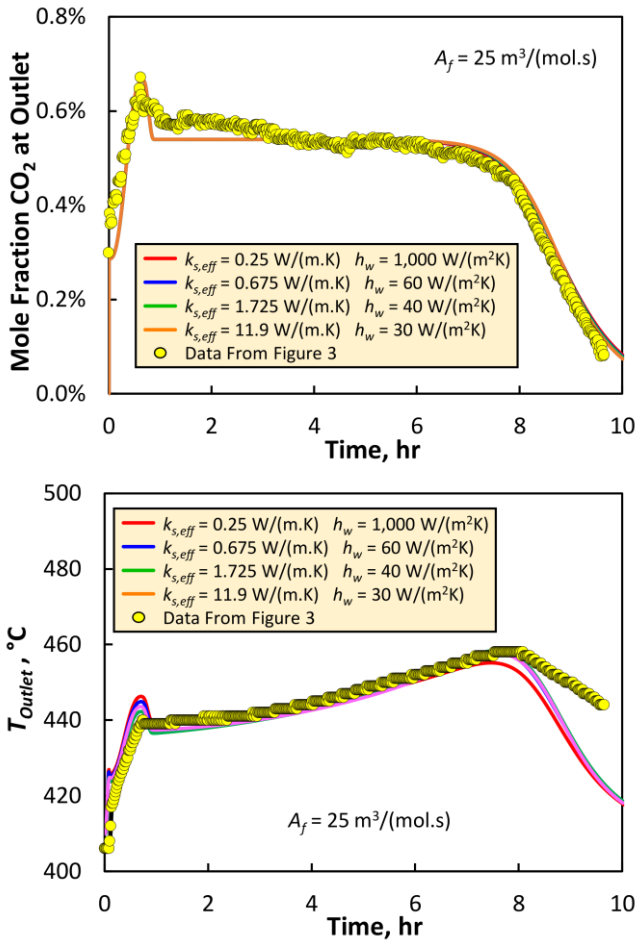

Figure 12. Experimental and modelled outlet temperature (top) and outlet CO_2 concentration (bottom) transient profiles for 2FBR simulations for the four best-fit parameter pairs found in this study.

Similar sweeps were computed for three other values of $k_{s,eff}$ spaced (roughly) logarithmically: 0.675, 1.725 and 11.9 W/(m.K). From these sweeps, the corresponding best-fit values of h_w were determined. The simulation results for the four best fit pairs are shown in Figure 12. Figure 13 shows a hypothetical locus of parameter pairs that can be used to generate additional parameter pairs for use in future, more refined studies.

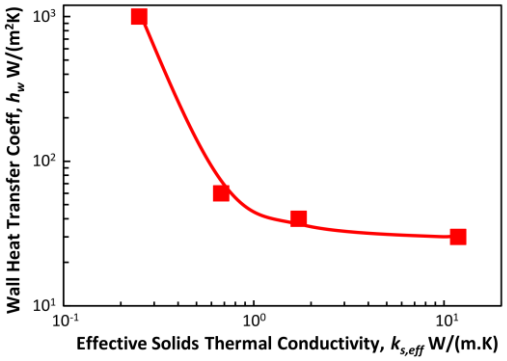

Figure 13. Hypothetical locus of best-fit parameter pairs from 2FBR simulations.

Figure S1 in the ESI shows the comparison of modelled and measured outlet temperature profiles using the predicted center point temperatures instead of the predicted area-averaged temperatures. These results, discussed in the ESI, suggest the averaged outlet temperatures are the better choice.

Notably, none of the 2FBR simulations eliminated the deviation between modelled and measured outlet temperature profiles visible at times on stream greater than 8 hours. One possible explanation is that the wall heat transfer conditions could be much different at the bottom of bed. If this were true and addressed correctly in the model, the extracted frequency factor could be different, since this time range represents the majority of the declining CO_2 region in the experimental data. However, there is no information at present to guide further model refinement in this direction.

TCPDU Pilot Scale Simulations

Four parametric sweeps were computed using the TCPDU pilot scale model for the four best-fit pairs of $k_{s,eff}$ and h_w shown in Figure 13. As shown in Table 6, each sweep consists of a 3x3 matrix of two flows: N_2 process diluent gas (mixed with process air as described below) and cooling air. Both flows are per catalyst bed and were fixed over the entire run. Unlike the lab-scale tests, the process gas was changed to upflow (i.e. reactor inlet at bottom) simply by setting the value of *CB* to -1.8879. This was decided after initial simulations showed that upflow led to shorter burnout periods, by allowing for greater initial airflow and faster ramping while still avoiding excessive overheating at startup. This upflow advantage is a consequence of the "downhill" coke profile and is not ubiquitous.

Table 6. TCPDU simulation parameter sweep. Flows are per catalyst bed.

N2 Flow, SLPM (410°C)	Cooling Air Flow, SLPM (30°C)		
	600	300	No Flow
400	Case 1	Case 2	Case 3
300	Case 4	Case 5	Case 6
200	Case 7	Case 8	Case 9

After some experimentation, the process airflow was fixed for all four sweeps. Initial airflow was set at 4 SLPM, increased over 2 hours to 12 SLPM, and held at 12 SLPM for the duration of the run. This corresponds to steady-state O_2 concentrations of 0.61, 0.81 and 1.2 v% for N_2 flows of 400, 300 and 200 SLPM, respectively. The inlet temperature of cooling air was fixed at 30°C, while inlet gas and initial bed temperatures were held at 410°C to maintain the bed temperature after upgrading and avoid thermal shock. Since the reactor wall was modelled with zero heat flux, no wall temperature specifications were needed. All 36 TCPDU simulations had carbon and oxygen mass balances between 99.5 and 100.5%. Small deviations from 100% are due

to small amounts of uncombusted carbon at the end of regeneration and/or minor errors in integration.

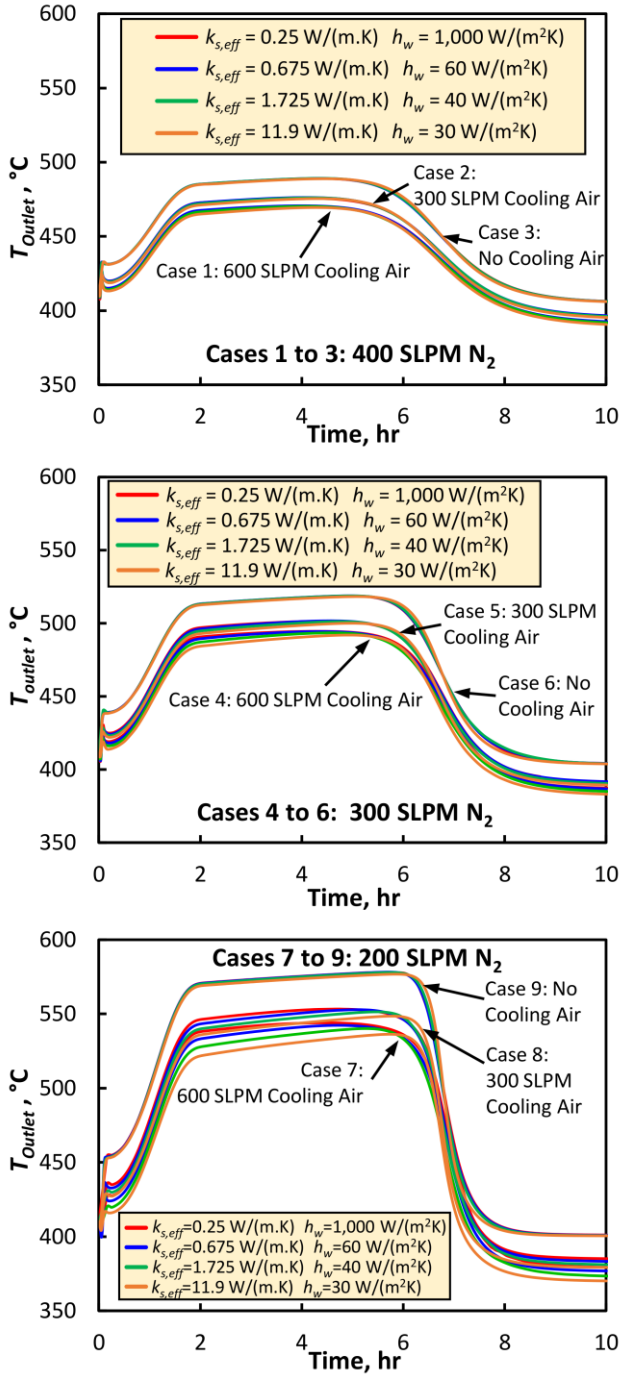

Figure 14. Predicted outlet temperature profiles for all 36 TCPDU simulations.

Figure 14 shows outlet temperature profiles for all 36 TCPDU simulations. Logically, convective cooling from through-bed process N_2 is much more effective for minimizing temperatures than conductive cooling using the embedded tubes. With 400 SLPM process N_2 flow, outlet temperatures are maintained below 500°C for all twelve combinations of heat transfer parameter pairs and cooling airflows. Conversely, with only 200 SLPM process N_2 flow, outlet temperatures above 500°C are predicted for all combinations of parameter pairs and cooling airflow. Differences due to heat transfer parameters increase with decreasing process N_2 flow and increasing cooling airflow. Corresponding tube wall heat flow profiles can be found in Figure S2 in the ESI. Total tube wall heat flow during the regeneration process is obtained by integrating these curves in time. Figure 15 shows the correlation between total tube wall heat flow and the three main variables: N_2 flow, cooling air flow and $k_{s,eff}$. Also shown is a simple power law regression model for these variables. As expected, cooling air flow is the dominant variable, accounting for 97% of the variance. Increasing flow of cooling air clearly has a diminishing return, as evident by the exponent of 0.533. Positive heat flows with zero cooling air flow correspond to axial heat conduction along the tube walls.

For reference, the total heat of combustion in this bed is slightly more than 16 MJ, so the maximum heat removal by the cooling tubes is slightly less than 50%.

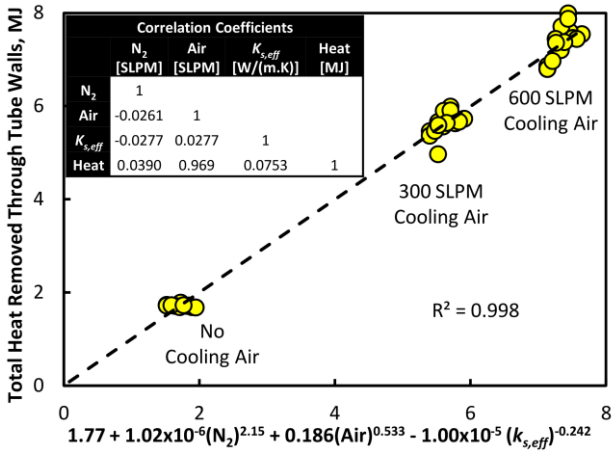

Figure 15. Total tube wall heat flow power law model and correlation coefficients. Gas flows are in units of SLPM.

Outlet temperatures and tube wall heat flows tell an incomplete story. It is instructive to look at thermal excursions inside the catalyst bed. Figure 16 shows the range in bed temperatures for the two extremes in heat transfer parameter pairs for case 7, which has the lowest process N_2 flow and highest cooling air flow. The combination of low $k_{s,eff}$ and high h_w results in the broadest temperature range, mainly because the low temperature boundary shifts downward. This lower boundary corresponds to pellets adjacent to tube walls. Notably, the maximum bed temperatures are higher than the average outlet bed temperatures across the entire high-temperature portion of the regeneration. Clearly, outlet temperatures alone cannot reveal the full extent of thermal excursions in the bed.

The top pair of graphs in Figure 17 show the maximum temperature gradient at any point in the bed, for the four parameter pairs. Two cases are shown: the low convection, high conduction case 7, and the high convection, low conduction case 3. In both cases, the combination of low $k_{s,eff}$

and high h_w leads to highest values of temperature gradient. For case 3, the highest gradients are around 300°C/cm; for case 7, the maximum values around 3,000°C/cm. In all cases, the maximum gradients are adjacent to the cooling tubes.

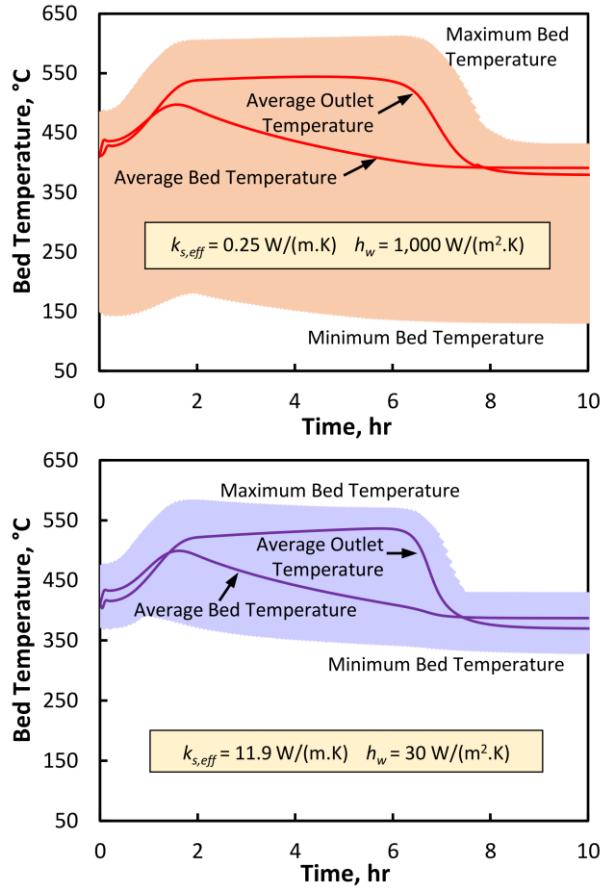

Figure 16. Temperature range over the entire catalyst bed, for the extreme pairs of thermal parameters in the case 7 simulations.

The bottom graphs in Figure 17 shows the same plots for maximum heating and cooling rates. Here, the low convection case 7 shows much larger maximum cooling rates for the three low conductivity parameter pairs, but for high convection case 3, all maximum heating and cooling rates are essentially identical. Since these are global maxima and minima, the geometric location of the point varies with time; in some cases there is considerable distance between the physical location of two adjacent points in time. For this reason, the curves appear very jagged.

Further insights into the temperature gradients for the two extreme cases in Figure 17 can be seen in the graphic images in Figure 18. These surface plots show the model results for the lowest thermal conductivity $k_{s,eff}$ = 0.25 W/(m.K) at a time on stream of 3 hrs. The largest gradients are located at the tube walls. There is a secondary region of smaller (but still high) gradients at the trailing edge of the combustion zone, where the freshly decarbonized bed is being cooled.

In total, the pilot scale model results show that the design concept put forth in this study faces significant risk of thermal catalyst damage and/or deactivation. The largest single uncertainty in this finding is the true value of effective thermal conductivity. While additional experimental results are needed to firm up this value, the assumption that the thermal conductivity is low, similar to values reported in the literature, suggests that substantial catalyst damage is likely. If this is true, the industrial viability of the proposed catalyst, bed and regeneration process is low.

Summary and Conclusions

Two finite element models for simulating oxidative regeneration of coked CFP catalyst in a packed bed reactor have been constructed. The first, bench scale model had a 2D axisymmetric geometry and was fitted to experimental regeneration data from a small (ca. 100 g) packed bed of catalyst. The starting coked catalyst had 25 w% carbon on catalyst (fresh catalyst basis) assumed to be distributed in an axial profile predicted by a recently published CFP upgrading kinetics model developed for the same catalyst and reactor. The model was fitted using two transient data sets: the average outlet temperature and the effluent CO_2 concentration. Three parameters were used in fitting the bench scale data: the carbon oxidation frequency factor, the effective solid thermal conductivity, and the wall heat transfer coefficient.

In combination with the assumed coke profile and activation energy, a reasonable value for the frequency factor of 25 m^3/(mol.s) was used to fit the experimental data in the region of declining CO_2 concentration near the end of the combustion period. The average outlet temperature data was matched using four values for effective solids thermal conductivity ranging from the bulk anatase value of 11.9 W/(m.K) to a very low (but typical in the literature) value of 0.25 W/(m.K), with two intermediate values spaced roughly logarithmically. For each conductivity value, a unique wall heat transfer coefficient was found to give the best match to average outlet temperature

The second, pilot scale model was used to examine a specific concept for scaling up the catalytic reactor by an overall factor of 60 using three parallel catalyst beds of 2 kg each. Each bed had three internal cooling tubes for flowing ambient air. Due to equipment limitations, the flow of process N_2 was capped at 400 SLPM per bed (1200 SLPM total) and the flow of cooling air was capped at 600 SLPM per bed (200 SLPM per tube, 1800 SLPM total). Equipment limitations also set a maximum pressure drop across the catalytic reactor system of 20 kPa. Also, regeneration time was capped at 10 hours.

This study has demonstrated that the design window for avoiding thermal excursions in the proposed combination of catalyst, bed and regeneration procedures is small, and possibly non-existent. Conduction of heat through the bed to the cooling tubes is much less effective for heat removal than convection of heat via process N_2 flowing through the bed. Not

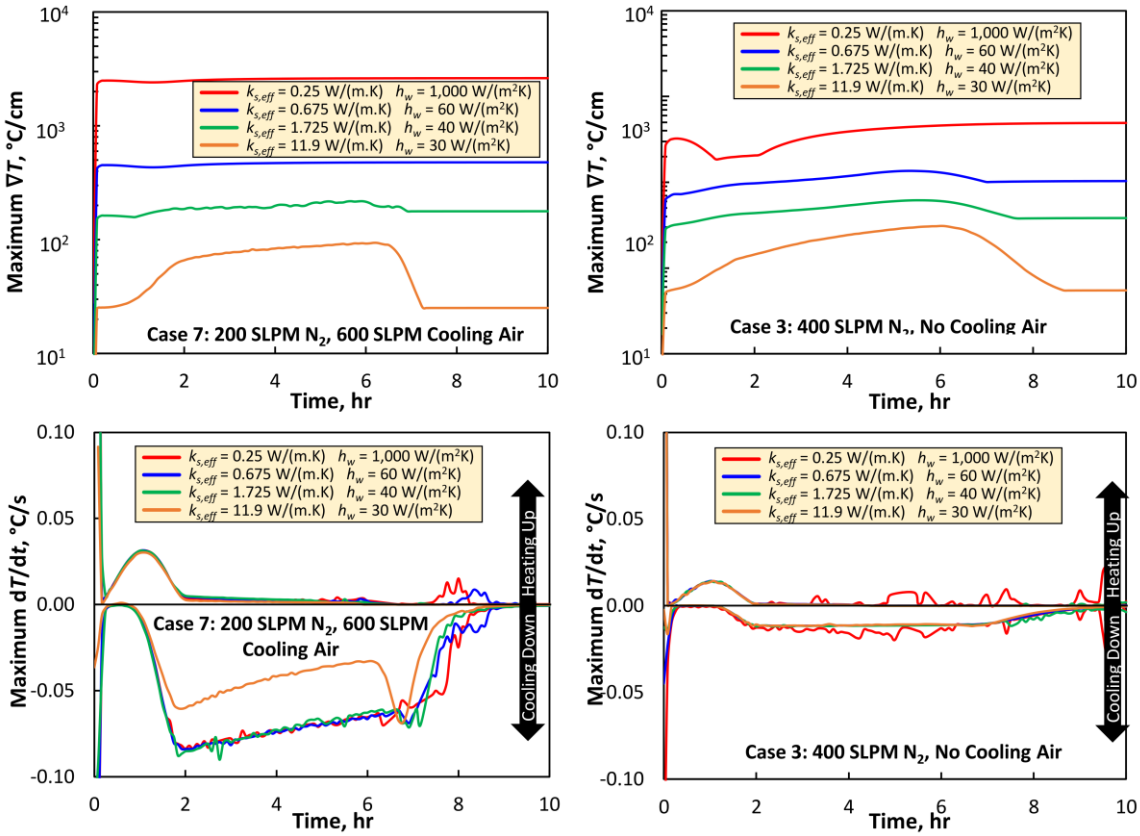

Figure 17. Top: maximum temperature gradient over the entire bed as a function of time, for cases 7 (left) and 3 (right). Note logarithmic scale. Bottom: maximum heating and cooling rates over the entire bed as a function of time, for cases 7 (left) and 3 (right).

surprisingly, high cooling airflow results in the highest near-tube temperature gradients, ranging from ca. 300°C/cm for the high process N_2, low cooling air case to ca. 3,000°C/cm for the low process N_2, high cooling air case. Assuming the catalyst pellets in this study have low effective thermal conductivities similar to literature examples, high temperatures and steep temperature gradients are almost certain to occur. These will prove excessive from the viewpoint of particle degradation and/or deactivation from active phase sintering.

Solutions to this problem are possible, but tricky. Internal cooling tubes will always show steep temperature gradients in their vicinity. Increasing cooling airflow will have diminishing returns; increasing the number and/or cross-sectional area of the tubes will increase the bed depth, pushing harder against the pressure drop limits. Increasing the process gas flow will also push against pressure drop limits.

Two alternate reactor configurations are being evaluated to retain the larger pellet size (compared to FCC-sized particles) and circumvent pressure drop and process gas flow limitations:

1. A radial flow reactor with high gas recycle rates and equivalent inlet airflows and gas purges (either with or without CO_2 scrubbing). Ideally the design would include heat exchangers to recoup the heat of combustion of the coke. Of course, in such a design, the cost of on-site manufacturing of N_2 using an ASU (air separation unit) needs to be compared to the cost of N_2 recycle and clean-up. Also, use of steam for carrier gas could reduce costs but would need to be proven.
2. A moving bed reactor with particle velocities much lower than those in FCC, such as a Continuous Catalyst Regeneration catalytic reformer like UOP's Platformer and other variants[31].

Also, options to increase the catalyst pellet size while maintaining catalyst activity, selectivity and lifetime are being investigated, which could benefit all of the design options.

On the whole, this modelling study suggests that the industrial relevance for the scale-up path represented by the proposed combination of catalyst, bed and regeneration procedure is low. However, this assessment is not free of uncertainty. The model is capable of reducing this uncertainty, provided the following issues are addressed:

- Effective solids thermal conductivities need to be measured experimentally.
- Coke profiles must be measured experimentally, using bed dissection techniques.
- Experiments to determine the effects of thermal excursions on catalyst degradation and deactivation should be carried out, along with measurements of the

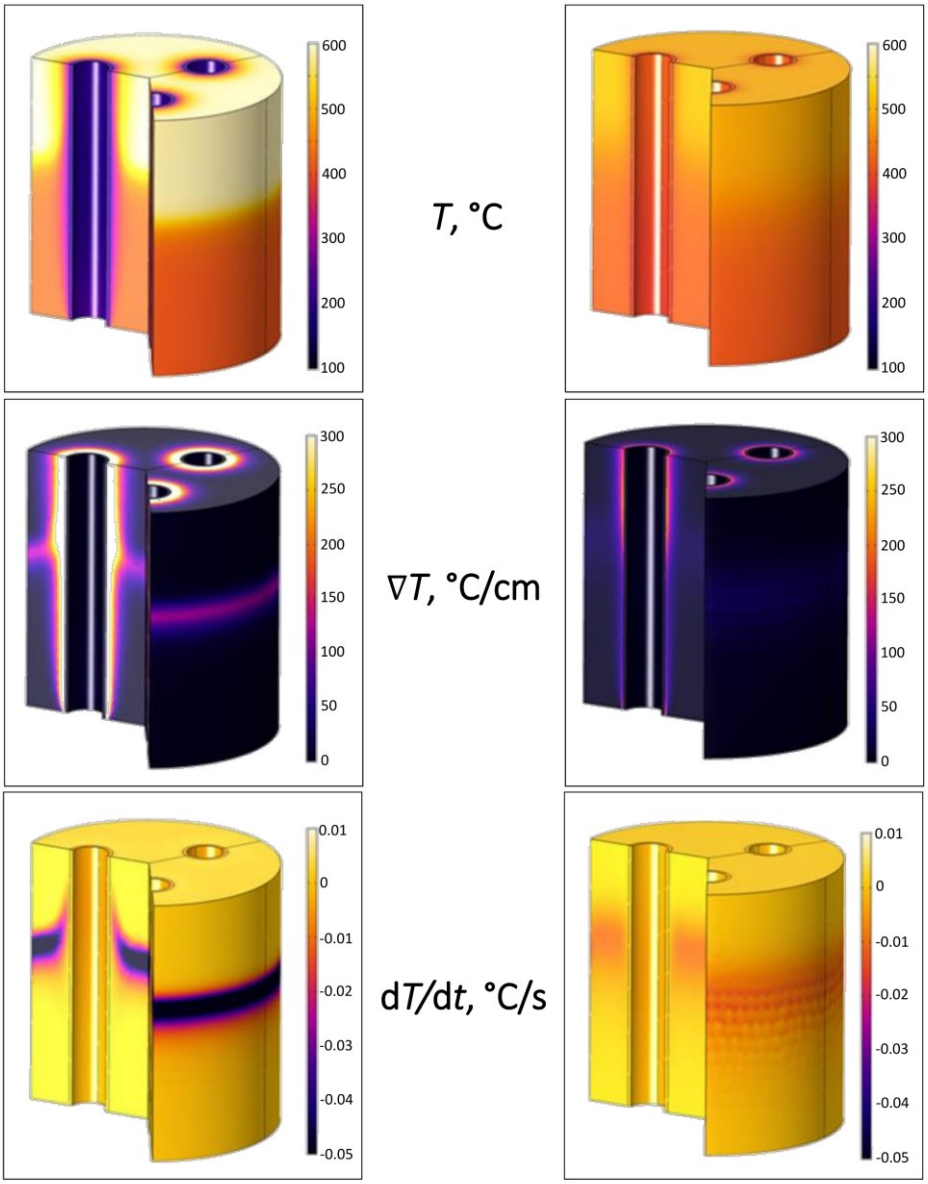

Figure 18. Surface plots for temperature (°C, top), temperature gradient (°C/cm, middle) and rate of temperature change (°C/s, bottom) at 3 hrs (10,800 s). Left: case 7, 200 SLPM N_2, 600 SLPM cooling air. Right: case 3, 400 SLPM N_2, no cooling air. Both simulations were computed using the minimum conductivity parameter pair: $k_{s,eff}$ = 0.25 W/(m.K) and h_w = 1,000 W/(m^2.K).

crush strength distributions of the particles. In the ideal case, crush strength of the particles should be measured at or near process temperatures using a hot-stage instrument.

Acknowledgements

This work was authored by Oak Ridge National Laboratory and the National Renewable Energy Laboratory under Contract DE-AC36-08-GO28308 in collaboration with the Consortium for Computational Physics and Chemistry (CCPC) and the Chemical Catalysis for Bioenergy Consortium (ChemCatBio). Funding was provided by the U.S. Department of Energy Office of Energy Efficiency and Renewable Energy's Bioenergy Technologies Office (BETO). The views expressed in the article do not necessarily represent the views of the DOE or the U.S. Government. The U.S. Government retains and the publisher, by accepting the article for publication, acknowledges that the U.S. Government retains a nonexclusive, paid-up, irrevocable, worldwide license to publish or reproduce the published form of this work, or allow others to do so, for U.S. Government purposes.

The authors would like to thank Scott Palmer, Rebecca Jackson, Kathleen Brown, and Matt Oliver for performing the 2FBR experiments.

References

1 Griffin MB, Iisa K, Wang H, Dutta A, Orton KA, French RJ, et al. Driving towards cost-competitive biofuels through catalytic fast pyrolysis by rethinking catalyst selection and reactor configuration. Energ Envir Sci. 2018;11(10):2904-18.
2 Iisa K, French RJ, Orton KA, Dutta A, Schaidle JA. Production of low-oxygen bio-oil via ex situ catalytic fast pyrolysis and hydrotreating. Fuel. 2017;207:413-22.
3 Wilson AN, Price MJ, Mukarakate C, Katahira R, Griffin MB, Dorgan JR, et al. Integrated Biorefining: Coproduction of Renewable Resol Biopolymer for Aqueous Stream Valorization. ACS Sustainable Chemistry & Engineering. 2017;5(8):6615-25.
4 Wilson AN, Dutta A, Black BA, Mukarakate C, Magrini K, Schaidle JA, et al. Valorization of aqueous waste streams from thermochemical biorefineries. Green Chemistry. 2019;21(15):4217-30.
5 Eschenbacher A, Saraeian A, Shanks BH, Jensen PA, Li C, Duus JØ, et al. Enhancing bio-oil quality and energy recovery by atmospheric hydrodeoxygenation of wheat straw pyrolysis vapors using Pt and Mo-based catalysts. Sustainable Energy & Fuels. 2020;4(4):1991-2008.
6 Griffin MB, Ferguson GA, Ruddy DA, Biddy MJ, Beckham GT, Schaidle JA. Role of the Support and Reaction Conditions on the Vapor-Phase Deoxygenation of m-Cresol over Pt/C and Pt/TiO2 Catalysts. ACS Catalysis. 2016;6(4):2715-27.
7 Wang K, Dayton DC, Peters JE, Mante OD. Reactive catalytic fast pyrolysis of biomass to produce high-quality bio-crude. Green Chemistry. 2017;19(14):3243-51.
8 Wan S, Pham T, Zhang S, Lobban L, Resasco D, Mallinson R. Direct catalytic upgrading of biomass pyrolysis vapors by a dual function Ru/TiO2 catalyst. AIChE Journal. 2013;59(7):2275-85.
9 Murugappan K, Mukarakate C, Budhi S, Shetty M, Nimlos MR, Román-Leshkov Y. Supported molybdenum oxides as effective catalysts for the catalytic fast pyrolysis of lignocellulosic biomass. Green Chemistry. 2016;18(20):5548-57.
10 Machado MA, He S, Davies TE, Seshan K, Teixeira da Silva V. Renewable fuel production from hydropyrolysis of residual biomass using molybdenum carbide-based catalysts: An analytical Py-GC/MS investigation. Catalysis Today. 2018;302:161-8.
11 Cross P, Wang K, Weiner J, Reid E, Peters J, Mante O, et al. Reactive Catalytic Fast Pyrolysis of Biomass Over Molybdenum Oxide Catalysts: A Parametric Study. Energ Fuel. 2020;34(4):4678-84.
12 Dutta A, Iisa MK, Talmadge M, Mukarakate C, Griffin MB, Tan EC, et al. Ex Situ Catalytic Fast Pyrolysis of Lignocellulosic Biomass to Hydrocarbon Fuels: 2019 State of Technology and Future Research. National Renewable Energy Laboratory (NREL), Golden, CO (United States); 2020.
13 Pecha MB, Iisa K, Griffin M, Mukarakate C, French R, Adkins B, et al. Ex situ upgrading of pyrolysis vapors over PtTiO 2: extraction of apparent kinetics via hierarchical transport modeling. Reaction Chemistry & Engineering 2020. DOI: 10.1039/d0re00339e.
14 Fahien R and Smith J. Mass transfer in packed beds, AIChE J. 1955; 28-35.
15 Dixon A. An improved correlation for overall heat transfer coefficient in packed beds. Chemical Engineering and Processing 35 (1996) 323-331.
16 Hickman D, Degenstein J and Ribeiro F. Fundamental principles of laboratory fixed bed reactor design. Current Opinion in Chemical Engineering 2016 (13) 109.
17 GradientCheck for Heterogeneous Catalysis v0.95, March 17, 2016. www.engineering.purdue.edu/~catalyst/gradientcheck
18 Loeb AL. Thermal conductivity: VIII, a theory of thermal conductivity of porous materials. Journal of the American Ceramic Society. 1954;37(2):96-9.
19 Masamune S, Smith J. Thermal Conductivity of Porous Catalyst Pellets. Journal of Chemical and Engineering Data. 1963;8(1):54-8.
20 Butt JB. Thermal conductivity of porous catalysts. AIChE Journal. 1965;11(1):106-12.
21 Pupeschi S, Knitter R, Kamlah M. Effective thermal conductivity of advanced ceramic breeder pebble beds. Fusion Engineering and Design. 2017;116:73-80.
22 Zou JH, Zhou ZJ, Wang FC, Zhang W, Dai ZH, Liu HF, et al. Modeling reaction kinetics of petroleum coke gasification with CO2. Chemical Engineering and Processing: Process Intensification. 2007;46(7):630-6.
23 In-situ regeneration guidelines. Albemarle Technical Information Bulletin HPC-13 1995.
24 J. Coulson JR. Chemical Engineering V1: Pergamon Press; 1991.
25 Welty J, Rorrer GL, Foster DG. Fundamentals of momentum, heat, and mass transfer: John Wiley & Sons; 2020.
26 Millington R, Quirk J. Permeability of porous solids. Transactions of the Faraday Society. 1961;57:1200-7.
27 Incropera FP, Dewitt DP, Bergman TL, Lavine AS. Fundamentals of heat and mass transfer, 2002. Hoboken, NJ: John Wiley. 1985:939-40.
28 Vendor specification sheet
29 https://www.azom.com/article.aspx?ArticleID=1179
30 "A multiscale 3D packed bed reactor", COMSOL application study 17019.
31 Lapinski M, Metro S, Pujado R and Moser M, Catalytic Reforming in Petroleum Refining. *Handbook of Petroleum Processing,* Springer International Publishing, 2015;255-258.